www.czasopisma.pan.pl PAN www.journals.pan.pl
Archives of Acoustics Vol. 46, No. 4, pp. 685–696 (2021), doi: 10.24425/aoa.2021.139645

Technical Note

Optimal Design for Multi-Diffuser Mufflers Using the Simulated Annealing Method

Min-Chie CHIU(1)*, Ho-Chih CHENG(2)

(1) *Department of Mechanical and Materials Engineering, Tatung University*
Taiwan, R.O.C.
*Corresponding Author e-mail: minchie.chiu@msa.hinet.net

(2) *Department of Intelligent Automation Engineering, Chung Chou University of Science and Technology*
Taiwan, R.O.C.

(*received March 24, 2021; accepted October 15, 2021*)

In this paper, a four-pole system matrix for evaluating acoustic performance (STL) is derived using a decoupled numerical method. During the optimization process, a simulated annealing (SA) method, which is a robust scheme utilized to search for the global optimum by imitating a physical annealing process, is used. Prior to dealing with a broadband noise, to recheck the SA method's reliability, the STL's maximization relative to a one-tone noise (400 Hz) is performed. To assure the accuracy of muffler's mathematical model, a theoretical analysis of one-diffuser muffler is also confirmed by an experimental data. Subsequently, the optimal results of three kinds of mufflers (muffler A: one diffuser; muffler B: two diffusers; muffler C: three diffusers) have also been compared. Results reveal that the acoustical performance of mufflers will increase when the number of diffusers installed at the muffler inlet increases.

Keywords: multiple diffuser; simulated annealing.

Nomenclature

This paper is constructed on the basis of the following notations:

T^*_{ij} – components of a four-pole transfer system matrix,
T_0 – initial temperature [°C],
S_i – section area at the i-th node [m^2],
T – temperature [°C],
c_0 – sound speed [m/s],
d_{Hi} – the diameter of the i-th diffuser's perforated hole [m],
D_i – diameter of the i-th tubes [m],
D_o – diameter of the outer tube [m],
f – frequency [Hz],
$iter$ – maximum number of iteration,
j – imaginary unit (= $\sqrt{-1}$),
k – wave number (= $\frac{\omega}{c_0}$),
kk – cooling rate,
L_{Ai}, L_{Bi} – lengths of non-perforated part for the i-th diffuser [m],
L_{Ci} – lengths of perforate part for the i-th perforated plug ducts [m],
L_o – total length of the muffler [m],
M_i – mean flow Mach number at the i-th node,
OBJ – objective function [dB],
$pb(T)$ – transition probability,
p_i – acoustic pressure at the i-th node [Pa],
Q – volume flow rate of a venting gas [m^3/s],
RT^{**}_1 – RT^{**}_{15} – design parameter for muffler C,
RT^{*}_1 – RT^{*}_{11} – design parameter for muffler B,
RT_1 – RT_7 – design parameter for muffler A,
STL – sound transmission loss [dB],
SWLI – unsilenced sound power level inside the muffler's inlet [dB],
SWLO – overall sound power level inside the muffler's output [dB],
TC_{ij} – components of a four-pole transfer matrix for an acoustical mechanism with a contracted perforated intruding tube,
TE_{ij} – components of a four-pole transfer matrix for an acoustical mechanism with an expanded perforated intruding tube,
t_i – the thickness of the i-th inner perforated tube [m],
TP_{ij} – components of a four-pole transfer matrix for an acoustical mechanism with a diffuser,
TS_{ij} – components of a four-pole transfer matrix for an acoustical mechanism with straight ducts,
u_i – acoustic particle velocity at the i-th node [m/s],

u_{ij} – acoustical particle velocity passing through a perforated hole from the i-th node to the j-th node [m/s],
V – mean flow velocity at the inner perforated tube [m/s],
ρ_i – acoustical density at the i-th node [m^3/s],
ξ – specific acoustical impedance of the inner perforated tube,
σ_i – a porosity of the i-th diffuser,
γ_i – i-th eigen value of $[\mathbf{H}]$,
$\gamma\gamma_i$ – i-th eigen value of $[\mathbf{HH}]$,
$[\Omega]_{4\times4}$ – model matrix formed by four sets of eigen vectors $\mathbf{\Omega}_{4\times1}$ of $[\mathbf{H}]_{4\times4}$,
$[\Omega\Omega]_{4\times4}$ – model matrix formed by four sets of eigen vectors $\mathbf{\Omega\Omega}_{4\times1}$ of $[\mathbf{HH}]_{4\times4}$.

1. Introduction

Enormous effort has been applied to the research of mufflers hybridized with perforated tubes. In dealing with high noise emitted from venting, a perforated plug tube installed at the muffler inlet is often used in today's factories. However, the acoustical performance of mufflers equipped with a one-ayer diffuser is still insufficient. In order to promote acoustic performance, a design and theoretical assessment on multiple perforated diffusers is then proposed. To overcome an exhaust noise emitted from a venting system, the assessment of perforated elements used in mufflers was initiated by Sullivan and Crocker (1978). They presented a series of theories and numerical techniques in decoupling the acoustical problems; however, the restrictions of non-flow and the problems' unstable solutions still existed. To overcome this drawback, Munjal (1987) and Peat (1988), then promulgated the generalized and numerical decoupling methods. Yet, the need to investigate the optimal muffler design within a constrained space was rarely tackled. In previous work (Yeh *et al.*, 2004; 2006; Chang *et al.*, 2004; 2005), the studies of optimal shape design in improving the performance of STL for various non-perforated mufflers were discussed. And, to depress the noise wave emitted from the machine casing, an optimally shaped one-layer close-fitting acoustical hood around the noise source was also presented (Chiu, 2014a). In addition, in order to eliminate pure tones that occurred in industrial plant, a hybrid model of broadband muffler conjugated with Helmholtz resonators was then established (Chiu, 2012); however, because of the drawback of dust accumulation inside the Helmholtz resonator, a new muffler design using side branch resonators that can easily remove the dust was adopted (Chiu, 2014b). Moreover, considering the high-order-wave effect, the acoustic performance of a one-chamber expansion muffler was explored using an eigen-function method (Chiu, Chang, 2014). In order to efficiently improve the performance of the noise control device, Chiu (2009a) analyzed a muffler equipped with a one-layer perforated diffuser using a SA method. Here, the reactive part designed in above muffler researches was one diffuser only. For a high noise emitted from a venting process, the acoustical performance of a one diffuser muffler is insufficient. Therefore, in order to increase the noise reduction of the mufflers, a new assessment of mufflers equipped with multi-layer perforated diffusers is presented. Here, three kinds of mufflers (muffler A; a one-diffuser muffler; muffler B; a two-diffuser muffler; muffler C; a three-diffuser muffler) are introduced. Also note: the numerical decoupling methods used in forming a four-pole matrix are in line with the simulated annealing method.

2. Mathematical model of the mufflers

Three kinds of multi-diffuser mufflers have been adopted for noise elimination in the diesel engine room shown in Fig. 1. Before the acoustical fields are analyzed, the acoustical fields and related outline dimensions of the mufflers are shown in Figs 2–4. As derived in previous work (Chiu, 2009a; 2013) and shown in Appendix, individual transfer matrices with respect to straight ducts, diffusers, and sudden expanded/contracted ducts are described below.

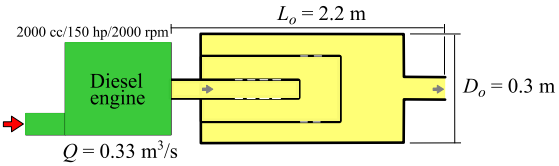

Fig. 1. Noise elimination for a space-constrained diesel engine.

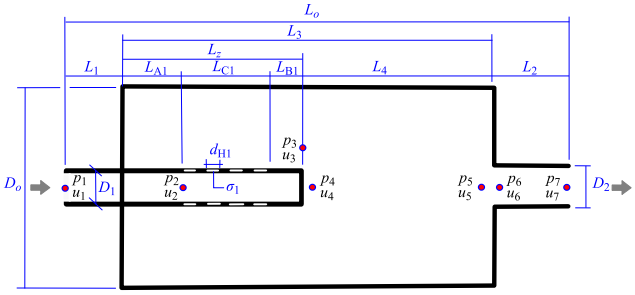

Fig. 2. The outline dimension of muffler A equipped with a one-layer diffuser.

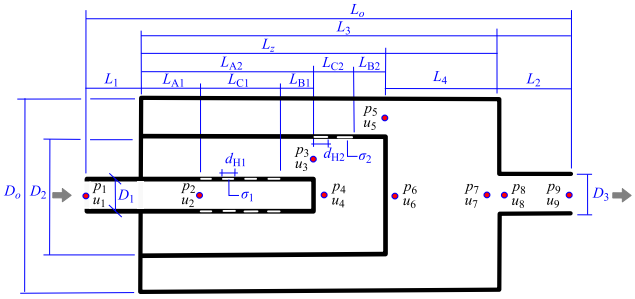

Fig. 3. The outline dimension of muffler B equipped with two layers of diffusers.

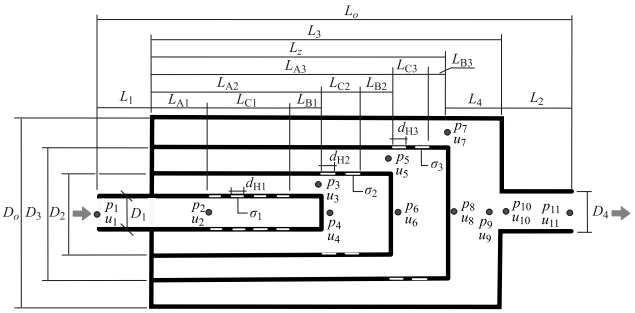

Fig. 4. The outline dimension of muffler C equipped with three layers of diffusers.

2.1. Muffler A (a one-diffuser muffler)

As seen in previous work (Chiu, 2009a; 2013), the four-pole matrix of the straight ducts (as shown in Fig. 2) between nodes 1 and 2 is

$$\begin{pmatrix} p_1 \\ \rho_o c_0 u_1 \end{pmatrix} = f_1(L_i, D_i, M_i) \cdot \begin{bmatrix} TS1_{1,1} & TS1_{1,2} \\ TS1_{2,1} & TS1_{2,2} \end{bmatrix} \begin{pmatrix} p_2 \\ \rho_o c_0 u_2 \end{pmatrix}. \quad (1)$$

The four-pole matrix between nodes 2 and 3 is

$$\begin{bmatrix} p_2 \\ \rho_o c_0 u_2 \end{bmatrix} = \begin{bmatrix} TP1_{1,1} & TP1_{1,2} \\ TP1_{2,1} & TP1_{2,2} \end{bmatrix} \begin{bmatrix} p_3 \\ \rho_o c_0 u_3 \end{bmatrix}. \quad (2)$$

Similarly, the four-pole matrix between nodes 3 and 4 is

$$\begin{bmatrix} p_3 \\ \rho_o c_0 u_3 \end{bmatrix} = \begin{bmatrix} TE1_{1,1} & TE1_{1,2} \\ TE1_{2,1} & TE1_{2,2} \end{bmatrix} \begin{bmatrix} p_4 \\ \rho_o c_0 u_4 \end{bmatrix}. \quad (3)$$

The four-pole matrix between nodes 4 and 5 is

$$\begin{pmatrix} p_4 \\ \rho_o c_0 u_4 \end{pmatrix} = f_2(L_i, D_i, M_i) \cdot \begin{bmatrix} TS2_{1,1} & TS2_{1,2} \\ TS2_{2,1} & TS2_{2,2} \end{bmatrix} \begin{pmatrix} p_5 \\ \rho_o c_0 u_5 \end{pmatrix}. \quad (4)$$

In addition, the four-pole matrix between nodes 5 and 6 is

$$\begin{bmatrix} p_5 \\ \rho_o c_0 u_5 \end{bmatrix} = \begin{bmatrix} TC1_{1,1} & TC1_{1,2} \\ TC1_{2,1} & TC1_{2,2} \end{bmatrix} \begin{bmatrix} p_6 \\ \rho_o c_0 u_6 \end{bmatrix}. \quad (5)$$

And, the four-pole matrix between nodes 6 and 7 is

$$\begin{pmatrix} p_6 \\ \rho_o c_0 u_6 \end{pmatrix} = f_3(L_i, D_i, M_i) \cdot \begin{bmatrix} TS3_{1,1} & TS3_{1,2} \\ TS3_{2,1} & TS3_{2,2} \end{bmatrix} \begin{pmatrix} p_7 \\ \rho_o c_0 u_7 \end{pmatrix}. \quad (6)$$

The total transfer matrix assembled by multiplication is

$$\begin{pmatrix} p_1 \\ \rho_o c_0 u_1 \end{pmatrix} = f_1(L_i, D_i, M_i) f_2(L_i, D_i, M_i) f_3(L_i, D_i, M_i) \cdot \begin{bmatrix} TS1_{1,1} & TS1_{1,2} \\ TS1_{2,1} & TS1_{2,2} \end{bmatrix} \begin{bmatrix} TP1_{1,1} & TP1_{1,2} \\ TP1_{2,1} & TP1_{2,2} \end{bmatrix} \begin{bmatrix} TE2_{1,1} & TE2_{1,2} \\ TE2_{2,1} & TE2_{2,2} \end{bmatrix} \cdot \begin{bmatrix} TS2_{1,1} & TS2_{1,2} \\ TS2_{2,1} & TS2_{2,2} \end{bmatrix} \begin{bmatrix} TC1_{1,1} & TC1_{1,2} \\ TC1_{2,1} & TC1_{2,2} \end{bmatrix} \begin{bmatrix} TS3_{1,1} & TS3_{1,2} \\ TS3_{2,1} & TS3_{2,2} \end{bmatrix} \cdot \begin{pmatrix} p_7 \\ \rho_o c_0 u_7 \end{pmatrix}. \quad (7)$$

A simplified form is expressed in a matrix as

$$\begin{pmatrix} p_1 \\ \rho_o c_0 u_1 \end{pmatrix} = \begin{bmatrix} T^*_{11} & T^*_{12} \\ T^*_{21} & T^*_{22} \end{bmatrix} \begin{pmatrix} p_7 \\ \rho_o c_0 u_7 \end{pmatrix}. \quad (8)$$

The sound transmission loss (STL) of muffler A is defined as (Munjal, 1987)

$$\mathrm{STL}_1(Q, f, \overline{X}_1) = 20 \log \left(\frac{|T^*_{11} + T^*_{12} + T^*_{21} + T^*_{22}|}{2} \right) + 10 \log \left(\frac{S_1}{S_7} \right), \quad (9)_1$$

$$\overline{X}_1 = (RT_1, RT_2, RT_3, RT_4, RT_5, RT_6, RT_7), \quad (9)_2$$

$$\begin{aligned} RT_1 &= L_3/L_o, & RT_2 &= L_Z/L_3, \\ RT_3 &= L_{C1}/L_Z, & RT_4 &= \sigma_1, \\ RT_5 &= d_{H1}, & RT_6 &= D_1/D_o, \\ RT_7 &= D_2/D_o. \end{aligned} \quad (9)_3$$

2.2. Muffler B (a two-diffuser muffler)

Similarly, as shown in Fig. 3, the acoustical four-pole matrices of straight elements between nodes 1–2 and nodes 6–7, and nodes 8–9 are the same as those shown in Eqs (1), (4), and (6). The acoustical four-pole matrices of expansion ducts between nodes 3–4 and nodes 5–6 are the same as those in Eq. (3). And, the four-pole matrix of a contraction duct between nodes 7–8 is the same as those illustrated in Eq. (5). As derived in Appendix, the four-pole matrices of two diffusers between nodes 2–3 and nodes 4–5 can be derived.

Consequently, the total transfer matrix assembled by multiplication is

$$\begin{pmatrix} p_1 \\ \rho_o c_o u_1 \end{pmatrix} = f_1(L_i, D_i, M_i) f_2(L_i, D_i, M_i) f_3(L_i, D_i, M_i) \cdot \begin{bmatrix} TS1_{1,1} & TS1_{1,2} \\ TS1_{2,1} & TS1_{2,2} \end{bmatrix} \begin{bmatrix} TP1_{1,1} & TP1_{1,2} \\ TP1_{2,1} & TP1_{2,2} \end{bmatrix} \begin{bmatrix} TE1_{1,1} & TE1_{1,2} \\ TE1_{2,1} & TE1_{2,2} \end{bmatrix} \cdot \begin{bmatrix} TP2_{1,1} & TP2_{1,2} \\ TP2_{2,1} & TP2_{2,2} \end{bmatrix} \begin{bmatrix} TE2_{1,1} & TE2_{1,2} \\ TE2_{2,1} & TE2_{2,2} \end{bmatrix} \begin{bmatrix} TS2_{1,1} & TS2_{1,2} \\ TS2_{2,1} & TS2_{2,2} \end{bmatrix} \cdot \begin{bmatrix} TC1_{1,1} & TC1_{1,2} \\ TC1_{2,1} & TC1_{2,2} \end{bmatrix} \begin{bmatrix} TS3_{1,1} & TS3_{1,2} \\ TS3_{2,1} & TS3_{2,2} \end{bmatrix} \begin{pmatrix} p_9 \\ \rho_o c_o u_9 \end{pmatrix}. \quad (10)$$

The sound transmission loss (STL) of muffler B is defined as (Munjal, 1987)

$$\mathrm{STL}_2(Q,f,\overline{X}_2) = 20\log\left(\frac{|T^*_{11}+T^*_{12}+T^*_{21}+T^*_{22}|}{2}\right) + 10\log\left(\frac{S_1}{S_9}\right), \tag{11}_1$$

$$\overline{X}_2 = (RT^*_1, RT^*_2, RT^*_3, RT^*_4, RT^*_5, RT^*_6, RT^*_7, RT^*_8, RT^*_9, RT^*_{10}, RT^*_{11}), \tag{11}_2$$

$$\begin{aligned} RT^*_1 &= L_3/L_o, & RT^*_2 &= L_Z/L_3 \\ RT^*_3 &= L_{A2}/L_Z, & RT^*_4 &= L_{C1}/L_{A2}, \\ RT^*_5 &= \sigma_1, & RT^*_6 &= d_{H1}, \\ RT^*_7 &= \sigma_2, & RT^*_8 &= d_{H2}, \\ RT^*_9 &= D_1/D_o, & RT^*_{10} &= D_2/D_o, \\ RT^*_{11} &= D_3/D_o. \end{aligned} \tag{11}_3$$

2.3. Muffler C (a three-diffuser muffler)

Likewise, as derived in Eqs (10), (11), and in Appendix, the total transfer matrix of the mufflers shown in Fig. 4 is assembled by multiplication as

$$\begin{pmatrix} p_1 \\ \rho_o c_o u_1 \end{pmatrix} = f_1(L_i,D_i,M_i) f_2(L_i,D_i,M_i) f_3(L_i,D_i,M_i) \cdot \begin{bmatrix} TS1_{1,1} & TS1_{1,2} \\ TS1_{2,1} & TS1_{2,2} \end{bmatrix} \begin{bmatrix} TP1_{1,1} & TP1_{1,2} \\ TP1_{2,1} & TP1_{2,2} \end{bmatrix} \begin{bmatrix} TE1_{1,1} & TE1_{1,2} \\ TE1_{2,1} & TE1_{2,2} \end{bmatrix} \cdot \begin{bmatrix} TP2_{1,1} & TP2_{1,2} \\ TP2_{2,1} & TP2_{2,2} \end{bmatrix} \begin{bmatrix} TE2_{1,1} & TE2_{1,2} \\ TE2_{2,1} & TE2_{2,2} \end{bmatrix} \begin{bmatrix} TP3_{1,1} & TP3_{1,2} \\ TP3_{2,1} & TP3_{2,2} \end{bmatrix} \cdot \begin{bmatrix} TE3_{1,1} & TE3_{1,2} \\ TE3_{2,1} & TE3_{2,2} \end{bmatrix} \begin{bmatrix} TS2_{1,1} & TS2_{1,2} \\ TS2_{2,1} & TS2_{2,2} \end{bmatrix} \begin{bmatrix} TC1_{1,1} & TC1_{1,2} \\ TC1_{2,1} & TC1_{2,2} \end{bmatrix} \cdot \begin{bmatrix} TS3_{1,1} & TS3_{1,2} \\ TS3_{2,1} & TS3_{2,2} \end{bmatrix} \begin{pmatrix} p_{11} \\ \rho_o c_o u_{11} \end{pmatrix}. \tag{12}$$

The sound transmission loss (STL) of muffler C can be defined as (Munjal, 1987)

$$\mathrm{STL}_3(Q,f,\overline{X}_3) = 20\log\left(\frac{|T^*_{11}+T^*_{12}+T^*_{21}+T^*_{22}|}{2}\right) + 10\log\left(\frac{S_1}{S_{11}}\right), \tag{13}_1$$

$$\overline{X}_3 = (RT^{**}_1, RT^{**}_2, RT^{**}_3, RT^{**}_4, RT^{**}_5, RT^{**}_6, RT^{**}_7, RT^{**}_8, RT^{**}_9, RT^{**}_{10}, RT^{**}_{11}, RT^{**}_{12}, RT^{**}_{13}, RT^{**}_{14}, RT^{**}_{15}), \tag{13}_2$$

$$\begin{aligned} RT^{**}_1 &= L_3/L_o, & RT^{**}_2 &= L_Z/L_3, \\ RT^{**}_3 &= L_{A3}/L_Z, & RT^{**}_4 &= L_{A2}/L_{A3}, \\ RT^{**}_5 &= L_{C1}/L_{A2}, & RT^{**}_6 &= \sigma_1, \\ RT^{**}_7 &= d_{H1}, & RT^{**}_8 &= \sigma_2, \\ RT^{**}_9 &= d_{H2}, & RT^{**}_{10} &= \sigma_3, \\ RT^{**}_{11} &= d_{H3}, & RT^{**}_{12} &= D_1/D_o, \\ RT^{**}_{13} &= D_2/D_o, & RT^{**}_{14} &= D_3/D_o, \\ RT^{**}_{15} &= D_4/D_o. \end{aligned} \tag{13}_3$$

2.4. Overall sound power level

The silent octave sound power level emitted from the k-th muffler's outlet is

$$\mathrm{SWLO}_{k-i} = \mathrm{SWLI}(f_i) - \mathrm{STL}_k(f_i), \tag{14}$$

where $\mathrm{SWLI}(f_i)$ is the original SWL at the inlet of a muffler (or pipe outlet), f_i is the relative octave band frequency, $\mathrm{STL}_k(f_i)$ is the k-th muffler's STL with respect to the relative octave band frequency (f_i), and SWLO_{k-i} is the silenced SWL at the outlet of the k-th muffler with respect to the relative octave band frequency.

Finally, the overall SWLO_k silenced by the k-th muffler (with a k-layer diffuser) at the outlet is

$$\begin{aligned} \mathrm{SWLO}_k &= 10\log\left\{\sum_{i=1}^{n} 10^{\mathrm{SWL}_{k-i}/10}\right\} \\ &= 10\log\Big\{10^{[\mathrm{SWLI}(f_1)-\mathrm{STL}_k(f_1)]/10} \\ &\quad + 10^{[\mathrm{SWLI}(f_2)-\mathrm{STL}_k(f_2)]/10} \\ &\quad + 10^{[\mathrm{SWLI}(f_3)-\mathrm{STL}_k(f_3)]/10} + \ldots \\ &\quad + 10^{[\mathrm{SWLI}(f_n)-\mathrm{STL}_k(f_n)]/10}\Big\}. \end{aligned} \tag{15}$$

2.5. Objective function

2.5.1. STL maximization for a tone (f) noise

The objective functions in maximizing the STL at a pure tone (f) are

$$\mathrm{OBJ}_{11} = \mathrm{STL}_1(Q,f,RT_1,RT_2,RT_3,RT_4,RT_5,RT_6,RT_7), \tag{16}_1$$

$$\mathrm{OBJ}_{12} = (Q,f,RT^*_1,RT^*_2,RT^*_3,RT^*_4,RT^*_5,RT^*_6,RT^*_7,RT^*_8,RT^*_9,RT^*_{10},RT^*_{11}), \tag{16}_2$$

$$\mathrm{OBJ}_{13} = (Q,f,RT^{**}_1,RT^{**}_2,RT^{**}_3,RT^{**}_4,RT^{**}_5,RT^{**}_6,RT^{**}_7,RT^{**}_8,RT^{**}_9,RT^{**}_{10},RT^{**}_{11},RT^{**}_{12},RT^{**}_{13},RT^{**}_{14},RT^{**}_{15}). \tag{16}_3$$

The related ranges of the parameters are $Q = 0.033$ m^3/s, $L_o = 2.2$ m, $D_o = 0.3$ m;

$$\begin{aligned} &RT_1 = [0.7, 0.9], && RT_2 = [0.7, 0.9], \\ &RT_3 = [0.5, 0.8], && RT_4 = [0.01, 0.1], \\ &RT_5 = [0.005, 0.015], && RT_6 = [0.1, 0.5], \\ &RT_7 = [0.1, 0.5]; \end{aligned} \tag{17}_1$$

$$\begin{aligned} &RT_1^* = [0.7, 0.9], && RT_2^* = [0.7, 0.9], \\ &RT_3^* = [0.5, 0.8], && RT_4^* = [0.2, 0.8], \\ &RT_5^* = [0.01, 0.1], && RT_6^* = [0.005, 0.015], \\ &RT_7^* = [0.01, 0.1], && RT_8^* = [0.005, 0.015], \\ &RT_9^* = [0.1, 0.3], && RT_{10}^* = [0.4, 0.8], \\ &RT_{11}^* = [0.1, 0.5], \end{aligned} \tag{17}_2$$

$$\begin{aligned} &RT_1^{**} = [0.7, 0.9], && RT_2^{**} = [0.7, 0.9], \\ &RT_3^{**} = [0.5, 0.8], && RT_4^{**} = [0.2, 0.8], \\ &RT_5^{**} = [0.2, 0.8], && RT_6^{**} = [0.01, 0.1], \\ &RT_7^{**} = [0.005, 0.015], && RT_8^{**} = [0.01, 0.1], \\ &RT_9^{**} = [0.005, 0.015], && RT_{10}^{**} = [0.01, 0.1], \\ &RT_{11}^{**} = [0.005, 0.015], && RT_{12}^{**} = [0.1, 0.3], \\ &RT_{13}^{**} = [0.4, 0.8], && RT_{14}^{**} = [0.7, 0.8], \\ &RT_{15}^{**} = [0.1, 0.5]. \end{aligned} \tag{17}_3$$

2.5.2. SWL minimization for a broadband noise

To minimize the overall SWL_T, the objective function is

$$\mathrm{OBJ}_{21} = \mathrm{SWL}_{T-1}(Q, f, RT_1, RT_2, RT_3, RT_4, RT_5, RT_6, RT_7), \tag{18}_1$$

$$\mathrm{OBJ}_{22} = \mathrm{SWL}_{T-2}(Q, f, RT_1^*, RT_2^*, RT_3^*, RT_4^*, RT_5^*, RT_6^*, RT_7^*, RT_8^*, RT_9^*, RT_{10}^*, RT_{11}^*), \tag{18}_2$$

$$\mathrm{OBJ}_{23} = \mathrm{SWL}_{T-3}(Q, f, RT_1^{**}, RT_2^{**}, RT_3^{**}, RT_4^{**}, RT_5^{**}, RT_6^{**}, RT_7^{**}, RT_8^{**}, RT_9^{**}, RT_{10}^{**}, RT_{11}^{**}, RT_{12}^{**}, RT_{13}^{**}, RT_{14}^{**}, RT_{15}^{**}). \tag{18}_3$$

3. Model check

Before performing the SA optimal simulation on mufflers, an accuracy check of the mathematical model on the one-chamber perforated plug muffler is performed using the experimental data from (Sullivan, 1979a; 1979b) and (Peat, 1988). As indicated in Fig. 5, accuracy between the theoretical and experimental data for a muffler equipped with a diffuser is in agreement. Therefore, the proposed fundamental mathematical models of mufflers equipped with concentric multi-layer diffusers are acceptable. Consequently, the model linked with the numerical method is applied to the shape optimization in the following section.

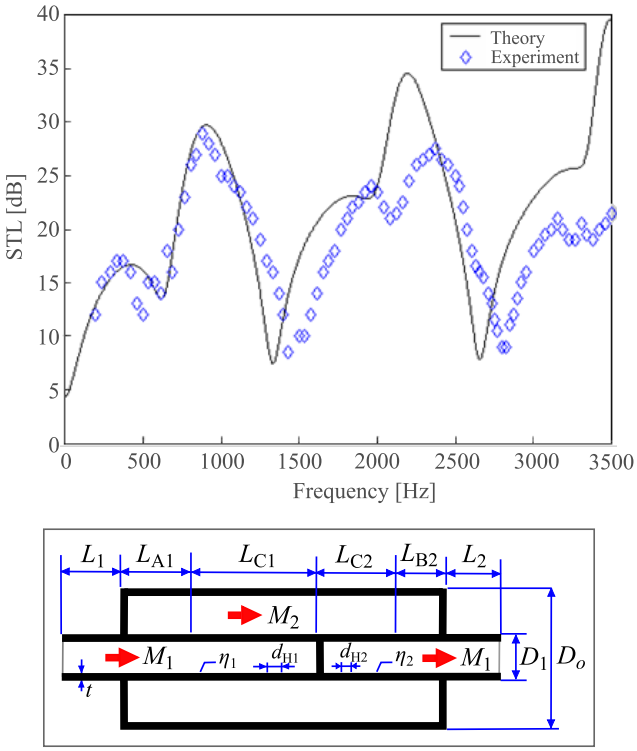

Fig. 5. Performance of a one-chamber perforated plug muffler with the mean flow ($M_1 = M_2 = 0.05$, $D_1 = 0.0493$ m, $D_o = 0.1016$ m, $L_{C1} = L_{C2} = 0.1286$ m, $L_1 = L_2 = 0.1$ m, $L_{A1} = L_{B2} = 0.0$ m, $t = 0.081$ m, $d_{H1} = d_{H2} = 0.00249$ m, $\eta_1 = \eta_2 = 0.037$). [Experimental data is from (Sullivan, 1979a; 1979b)].

4. Parameter sensitivity analysis

In order to understand the influence of the design parameters for a muffler with multi-layer diffuser, an investigation of the acoustical influence with respect to the design parameters in muffler B is exemplified and assessed. By conducting the design parameters into Eq. (11), the resulting STLs with respect to the design parameters RT_1^*–RT_{11}^* have be explored and shown in Figs 6–9. As indicated in Figs 6–9, the STL is influenced by the design parameters RT_1^*–RT_{11}^*. As can be seen in Fig. 8 and Fig. 9, the STL is inversely proportional to both the perforated hole's diameter (d_{H2} in the 2nd diffuser) and the outlet's diameter (D_3). Obviously, all the design parameters are essential during the optimization process. Therefore, the design parameters RT_1–RT_7 in muffler A, the design parameters RT_1^*–RT_{11}^* in muffler B, and the design parameters RT_1^{**}–RT_{15}^* in muffler C are recognized to be the most important design parameters and will be considered to adopt in the following muffler design work.

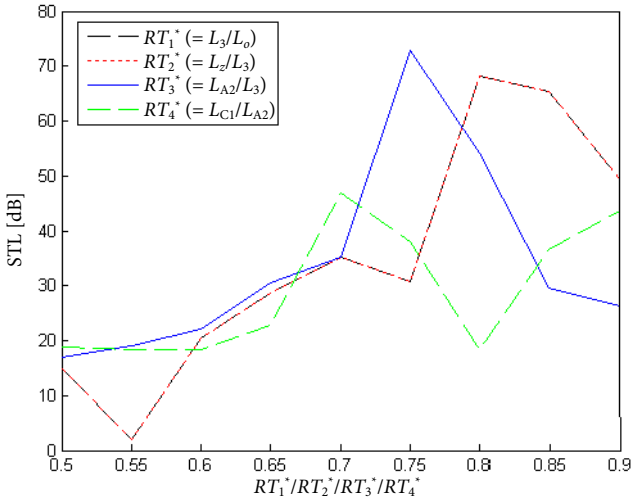

Fig. 6. The STL with respect to parameter $RT_1^*(L_3/L_o)$, RT_2^* (L_z/L_3), RT_3^* (L_{A2}/L_3), and RT_4^* (L_{C1}/L_{A2}) at 400 Hz (muffler B).

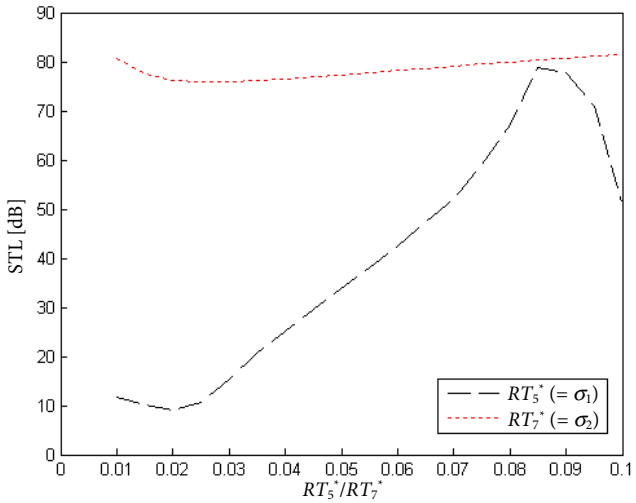

Fig. 7. The STL with respect to parameter RT_5^* (σ_1) and RT_7^* (σ_2) at 400 Hz (muffler B).

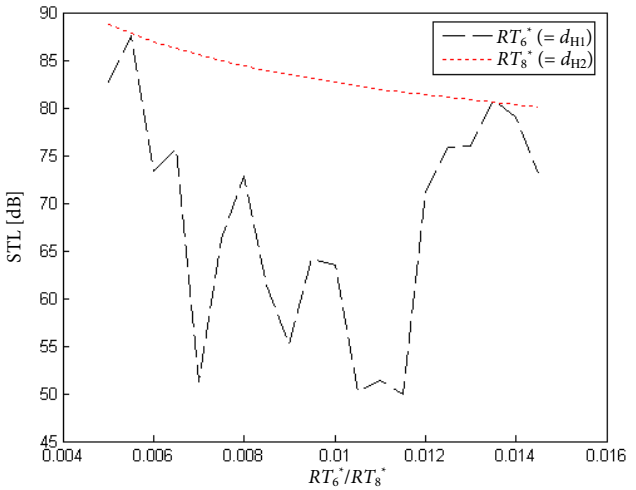

Fig. 8. The STL with respect to parameter RT_6^* (d_{H1}) and RT_8^* (d_{H2}) at 400 Hz (muffler B).

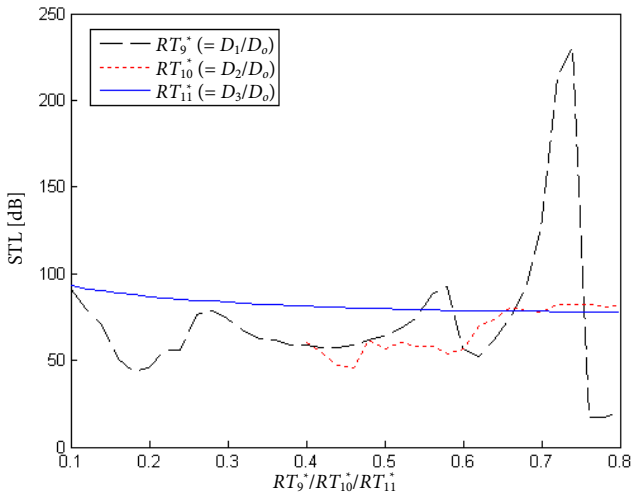

Fig. 9. The STL with respect to parameter RT_9^* (D_1/D_o), RT_{10}^* (D_2/D_o), and RT_{11}^* (D_3/D_o) at 400 Hz (muffler B).

5. Muffler design

To reduce the huge venting noise emitted from the diesel engine's outlet, three kinds of mufflers equipped with multi-layer diffusers (mufflers A–C) are adopted. To obtain a best acoustical performance within a fixed space, numerical assessments linked to a SA optimizer are applied. As indicated in Fig. 1, a space-constrained diesel engine with 150 hp and 2000 RPM has a venting flow rate Q of 0.033 m^3/s. According to the formula from (Bie, Hansen, 1988), an overall sound power level (SWL) emitted from the diesel engine at the exhaust outlet tube is predicted as

$$\mathrm{SWL} = 120 + 10\log_{10} kw - (l_{\mathrm{ex}}/1.2), \tag{19}$$

where l_{ex} = 0.3 m is the length of the exhaust outlet tube. The primary spectrum of the diesel engine's exhaust SWL inside the pipe outlet (muffler's inlet) is calculated and shown in Table 1. As indicated in Table 1, the sound power level (SWL) inside the diesel engine's outlet reaches 128.7 dB(A).

Table 1. Unsilenced SWL of an engine inside a duct outlet.

Frequency [Hz]	125	250	500	1000	2000	overall
SWL = 120 + 10 log$_{10}$ kw – (l_{ex}/1.2) [dB]	140.2	140.2	140.2	140.2	140.2	
Spectrum correction [dB]	–3	–7	–15	–19	–25	
A-weighted	–16	–9	–3	–0	+1	
SWLO [dB(A)]	121.2	124.2	122.2	121.2	116.2	128.7

Before the muffler optimization is performed, a reliability check of the SA method by the maximization of the STL at a targeted tone (400 Hz) is performed. As shown in Fig. 1, the available space for a muffler is 0.3 m in width, 0.3 m in height, and 2.2 m in length. The corresponding OBJ functions, space constraints, and the ranges of design parameters are summarized in Eqs (16)–(18).

6. Simulated annealing method

Evolutionary algorithms (EAs), which search for appropriate global solutions in engineering problems, have been widely discussed for two decades. Here, simulated annealing (SA) is recognized as one of the best stochastic search method. Because there is no need to choose starting data that is necessary for the classical gradient methods of EPFM, IPFM and FDM (Chang *et al.*, 2005), the SA becomes convenient during the numerical assessment.

Simulated annealing (SA) was first introduced by Metropolis *et al.* (1953) and further developed by Kirkpatrick *et al.* (1983). According to the philosophy of SA, the desired objective function is to bring the system from an arbitrary initial state to one with minimum possible energy. Because of annealing, which is a heating process that stabilizes a metal's temperature while slowing cooling it, the particles remain close to the minimum energy state. In order to emulate the SA's evolution, a new random solution (X') is chosen from the neighborhood of the current solution. If, conceivably, there is a negative change in the objective function ($\Delta F \le 0$), the new solution will be recognized as the new current solution. If, conversely, there is not a negative change, the probability ($pb(X')$) of a transition to the new state will be calculated using the Boltzmann factor ($pb(X') = \exp(\Delta F/CT)$) where C and T are the Boltzmann constant and the current temperature

$$pb(X') = \begin{cases} 1, & \Delta F \le 0, \\ \exp\left(\frac{-\Delta F}{CT}\right), & \Delta F > 0, \end{cases} \qquad (20)$$
$$\Delta F = F(X') - F(X).$$

For the purpose of escaping from the local optimum, SA also permits movement that results in inferior solutions (uphill movement). Hence, if the transition property ($pb(X')$) is greater than a random number of rand(0,1), the new inferior solution, which results in a higher energy condition, will be accepted; if not, it will be rejected. Each successful substitution of the new current solution will conduct to the decay of the current temperature as

$$T_{\text{new}} = kk \cdot T_{\text{old}}, \qquad (21)$$

where kk is the cooling rate. This process will be repeated until the preset *iter* of the outer loop is reached (Chiu, 2009b; 2010a; 2010b).

7. Results and discussion

7.1. Results

To achieve good optimization, two kinds of SA parameters including kk (cooling rate) and *iter* (maximum iteration) are varied step by step:

$$kk(0.90, 0.92, 0.94, 0.96, 0.98);$$
$$iter(50, 100, 200, 2000, 20000).$$

Two results of optimization (one, pure tone noises used for the SA's accuracy check; and the other, a broadband noise occurring in a diesel engine outlet) are described below.

7.1.1. Pure tone noise optimization

Before dealing with a broadband noise for muffler A–C, the STLs maximization for muffler B with respect to a one-tone noise (400 Hz) is introduced for a reliability check on the SA method. By using Eq. $(16)_2$, the maximization of the STL with respect to muffler B (a muffler equipped with two-layer diffusers) at the specified pure tone (400 Hz) was performed first. As indicated in Table 2, optimal design data can

Table 2. Optimal STL for muffler A (equipped with two layers of diffusers) at various SA parameters (targeted tone of 400 Hz).

SA parameter		Design parameters											Result
iter	*kk*	RT_1^*	RT_2^*	RT_3^*	RT_4^*	RT_5^*	RT_6^*	RT_7^*	RT_8^*	RT_9^*	RT_{10}^*	RT_{11}^*	$\text{STL}_{500\text{ Hz}}$ [dB]
50	0.90	0.8529	0.8529	0.7294	0.6588	0.07882	0.012650	0.07882	0.012650	0.2529	0.7059	0.4059	44.22
50	0.92	0.8579	0.8579	0.7369	0.6738	0.08107	0.012900	0.08107	0.012900	0.2579	0.7159	0.4159	44.87
50	0.94	0.8783	0.8783	0.7674	0.7348	0.09022	0.013910	0.09022	0.013910	0.2783	0.7565	0.4565	59.17
50	0.96	0.7123	0.7123	0.5185	0.2370	0.01554	0.005616	0.01554	0.005616	0.1123	0.4246	0.1246	66.76
50	0.98	0.7177	0.7177	0.5265	0.2531	0.01796	0.005885	0.01796	0.005885	0.1177	0.4354	0.1354	62.40
100	0.96	0.7084	0.7084	0.5126	0.2252	0.01378	0.005420	0.01378	0.005420	0.1084	0.4168	0.1168	72.07
200	0.96	0.8714	0.8714	0.7571	0.7143	0.08714	0.013570	0.08714	0.013570	0.2714	0.7428	0.4428	81.70
2000	0.96	0.7000	0.7000	0.5001	0.2001	0.01002	0.005002	0.01002	0.005002	0.1000	0.4001	0.1001	91.32
20000	0.96	0.7000	0.7000	0.5001	0.2001	0.01002	0.005002	0.01002	0.005002	0.1000	0.4001	0.1001	91.32

be obtained at the eighth set of the SA parameters at (*kk*, *iter*) = (0.96, 2000). Using the optimal design in a theoretical calculation, the optimal STL curves with respect to various SA parameters (*kk*, *iter*) are plotted and depicted in Figs 10 and 11. As revealed in Figs 10 and 11, the STL is precisely maximized at the

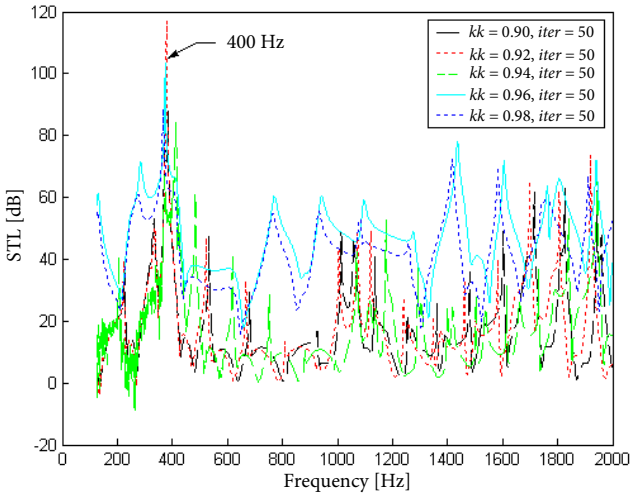

Fig. 10. STL with respect to various *kk* (muffler B: target tone = 400 Hz).

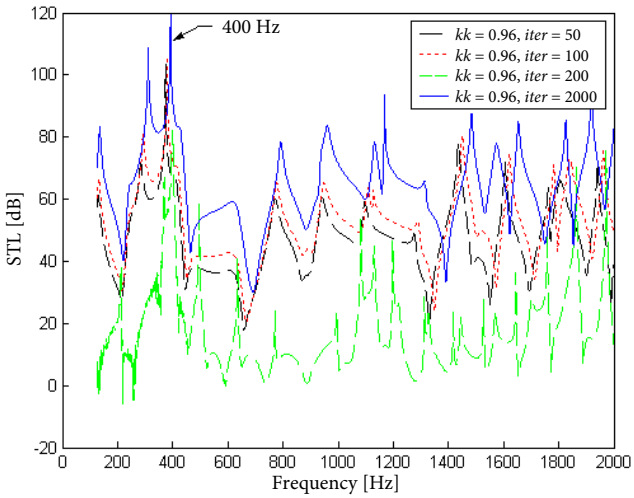

Fig. 11. STL with respect to various *iter* (muffler B: target tone = 400 Hz).

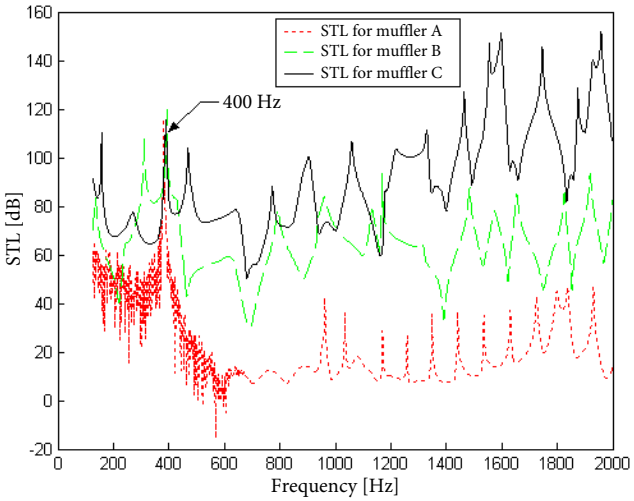

Fig. 12. Comparison of the optimal STLs of three kinds of mufflers (mufflers A, B, and C) optimized at a targeted tone of 400 Hz.

desired frequency of 400 Hz. Therefore, the SA optimizer is reliable in the optimization process. Using the same SA parameters (*kk*, *iter*) in mufflers A and C, the optimal STL curves of mufflers A–C are obtained in Table 3 and plotted in Fig. 12. As illustrated in Table 3, the STLs of mufflers A–C at 400 Hz reach 64.92 dB, 91.32 dB, and 95.5 dB, respectively.

7.1.2. Broadband noise optimization

Similarly, adopting the same SA parameters of (*kk*, *iter*) = (0.96, 2000) and minimizing the broadband noise at SWL_{T-1}, SWL_{T-2}, and SWL_{T-3} (mufflers A–C), the resulting design parameters are obtained and shown in Table 4. Using the optimal design parameters in a theoretical calculation, an optimal STL curves with respect to various mufflers A–C are plotted and depicted in Fig. 13. As illustrated in Table 4 and Fig. 13, the resultant sound power levels with respect to three kinds of mufflers have been reduced from 128.7 dB(A) to 102.2 dB(A), 78.34 dB(A), and 66.75 dB(A).

Table 3. Optimal design data for three kinds of mufflers (mufflers A–C) (at a targeted tone of 400 Hz) (*kk* = 0.96, *iter* = 2000).

Muffler	Design parameters											Result
A	RT_1	RT_2	RT_3	RT_4	RT_5	RT_6	RT_7					$STL_{400\ Hz}$ [dB]
	0.8998	0.8998	0.7997	0.09990	0.01499	0.4995	0.4995					64.92
B	RT_1^*	RT_2^*	RT_3^*	RT_4^*	RT_5^*	RT_6^*	RT_7^*	RT_8^*	RT_9^*	RT_{10}^*	RT_{11}^*	$STL_{400\ Hz}$ [dB]
	0.7000	0.7000	0.5001	0.2001	0.01002	0.005002	0.01002	0.005002	0.1000	0.4001	0.1001	91.32
C	RT_1^{**}	RT_2^{**}	RT_3^{**}	RT_4^{**}	RT_5^{**}	RT_6^{**}	RT_7^{**}	RT_8^{**}	RT_9^{**}	RT_{10}^{**}	RT_{11}^{**}	$STL_{400\ Hz}$ [dB]
	0.7000	0.7000	0.5001	0.2001	0.2001	0.01002	0.0050	0.01002	0.0050	0.01002	0.005002	95.5
	RT_{12}^{**}	RT_{13}^{**}	RT_{14}^{**}	RT_{15}^{**}								
	0.1000	0.4000	0.7000	0.1001								

Table 4. Optimal design data for three kinds of mufflers (mufflers A–C) (broadband noise) (kk = 0.96, $iter$ = 2000).

Muffler	Design parameters											Result
A	RT_1	RT_2	RT_3	RT_4	RT_5	RT_6	RT_7					SWL_T [dB(A)]
	0.7063	0.7063	0.5094	0.01281	0.005313	0.1125	0.1125					102.2
B	RT_1^*	RT_2^*	RT_3^*	RT_4^*	RT_5^*	RT_6^*	RT_7^*	RT_8^*	RT_9^*	RT_{10}^*	RT_{11}^*	SWL_T [dB(A)]
	0.7063	0.7063	0.5094	0.2188	0.01281	0.005313	0.01281	0.005313	0.1063	0.4125	0.1125	78.34
C	RT_1^{**}	RT_2^{**}	RT_3^{**}	RT_4^{**}	RT_5^{**}	RT_6^{**}	RT_7^{**}	RT_8^{**}	RT_9^{**}	RT_{10}^{**}	RT_{11}^{**}	SWL_T [dB(A)]
	0.7056	0.7056	0.5084	0.2168	0.2168	0.01251	0.00527	0.01251	0.0053	0.01251	0.005279	66.75
	RT_{12}^{**}	RT_{13}^{**}	RT_{14}^{**}	RT_{15}^{**}								
	0.1056	0.4056	0.7028	0.1112								

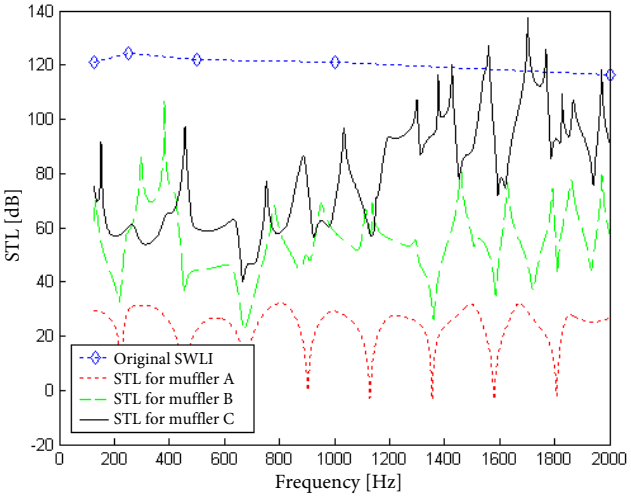

Fig. 13. Comparison of the optimal STLs of three kinds of mufflers (mufflers A, B, and C) and the original SWL (broadband noise elimination).

7.2. Discussion

In order to achieve an optimally shaped muffler, the selection of design parameters is essential. An investigation of the design parameters' influence on muffler B is introduced. The acoustical influence with respect to design parameters RT_1^*–RT_{11}^* are shown in Figs 6–9. Figures 6–9 indicate that the STL is tightly related to the design parameters RT_1^*–RT_{11}^*. Therefore, the design parameters RT_1–RT_7 in muffler A, the design parameters RT_1^*–RT_{11}^* in muffler B, and the design parameters RT_1^{**}–RT_{15}^{**} in muffler C are selected as the optimization parameters.

To achieve a sufficient optimization, the selection of an appropriate SA parameter set is essential. As indicated in Table 2, the best SA set for muffler B at the targeted pure tone of 400 Hz has been found at the eighth set. The related STL curves with respect to various SA parameters are plotted in Figs 10 and 11. Figures 10 and 11 reveal that the predicted maximal value of the STL is precisely located at the desired frequency. Similarly, in dealing with pure tone noise (400 Hz) in muffler A and muffler C, the profiles shown in Fig. 12 indicate that the maximum STLs of the mufflers are also located at the specified frequency.

In dealing with broadband noise, the acoustical performance for three kinds of mufflers (mufflers A, B, and C) is shown in Table 4 and Fig. 13. As can be observed in Table 4, the overall sound transmission loss of a muffler equipped with one perforated diffuser (muffler A) reaches 26.5 dB. And, the overall sound transmission losses of a muffler equipped with two perforated diffusers (muffler B) reaches 50.5 dB. Furthermore, the overall STL of a muffler equipped with three perforated diffusers (muffler C) arrives at 61.9 dB. It is obvious that the acoustical performance of a muffler equipped with diffusers installed at the muffler inlet will increase if the number of diffusers increases.

8. Conclusion

It has been shown that mufflers hybridized with multiple perforated diffusers can be efficiently optimized within a limited space by using a decoupling technique, a plane wave theory, a four-pole transfer matrix, and an SA optimizer. As indicated in Table 2 and Figs 10 and 11, two kinds of SA parameters (kk and $iter$) play essential roles in the solution's accuracy during SA optimization. Figures 10, 11, and 12 indicate that the tuning ability established by adjusting design parameters in mufflers A–C is reliable. Moreover, the appropriate design parameters for three kinds of mufflers hybridized with multiple perforated diffusers (mufflers A–C) have been assessed. Consequently, as indicated in Table 4, the resulting SWL_T with respect to these mufflers are 102.2 dB(A), 78.3 dB(A), and 66.8 dB(A). Obviously, the muffler hybridized with more perforated diffusers is superior to the mufflers equipped with fewer perforated diffusers.

Appendix
Transfer matrix of two perforated diffusers

As indicated in Fig. 14, the two diffusers are composed of two concentric perforated tubes which are closed at the end. The continuity equations and mo-

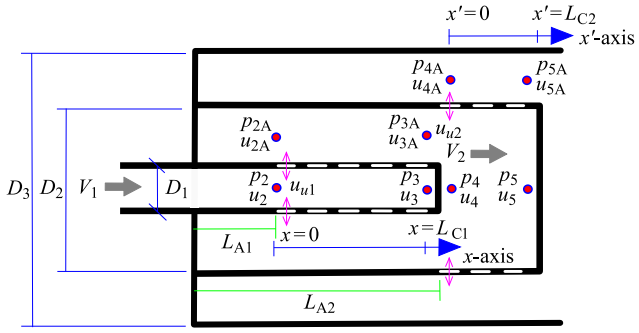

Fig. 14. The acoustical mechanism of a muffler equipped with two layers of perforated diffusers.

mentum equations of the first perforated diffuser with respect to the inner and outer tubes at nodes 2 and 2A are

- first inner tube:
  continuity equation (SULLIVAN, CROCKER, 1978):

$$V\frac{\partial \rho_2}{\partial x}+\rho_o\frac{\partial u_2}{\partial x}+\frac{4\rho_o}{D_1}u_{u_1}+\frac{\partial \rho_2}{\partial t}=0; \tag{22}$$

  momentum equation:

$$\rho_o\left(\frac{\partial}{\partial t}+V_1\frac{\partial}{\partial x}\right)u_2+\frac{\partial p_2}{\partial x}=0; \tag{23}$$

- first outer tube:
  continuity equation

$$\rho_o\frac{\partial u_{2A}}{\partial x}-\frac{4D_1\rho_o}{D_2^2-D_1^2}u_{u_1}+\frac{\partial \rho_{2A}}{\partial t}=0, \tag{24}$$

  momentum equation

$$\rho_o\frac{\partial u_{2A}}{\partial t}+\frac{\partial p_{2A}}{\partial x}=0. \tag{25}$$

Assuming that the acoustic wave is a harmonic motion under the isentropic processes in ducts, then

$$\begin{aligned} p(x,t)&=P(x)\cdot e^{j\omega t},\\ P(x)&=\rho(x)\cdot c_0^2. \end{aligned} \tag{26}$$

Plugging Eqs (26) into Eqs (22)–(25) and doing a rearrangement yields

$$\rho_o c_0\frac{\mathrm{d}u_2}{\mathrm{d}x}=-\left[jkp_2+\frac{V_2}{c_0}\cdot\frac{\mathrm{d}p_2}{\mathrm{d}x}+\frac{4\cdot(p_2-p_{2A})}{D_1\varsigma_1}\right], \tag{27}$$

$$\rho_o c_0\frac{\mathrm{d}u_{2A}}{\mathrm{d}x}=-\left[jkp_{2A}-\frac{4D_1\cdot(p_2-p_{2A})}{(D_2^2-D_1^2\varsigma_1)}\right], \tag{28}$$

$$\rho_o c_0\left(jku_2+\frac{V_1}{c_0}\cdot\frac{\mathrm{d}u_2}{\mathrm{d}x}\right)=-\frac{\mathrm{d}p_2}{\mathrm{d}x}, \tag{29}$$

$$j\rho_o c_0 ku_{2A}=-\frac{\mathrm{d}p_{2A}}{\mathrm{d}x}. \tag{30}$$

Eliminating u_5 and u_{5A} yields

$$\left[\left(1-M_1^2\right)\frac{\mathrm{d}^2}{\mathrm{d}x^2}-2jM_1k\frac{\mathrm{d}}{\mathrm{d}x}+k^2\right]p_2-\frac{4}{D_1\varsigma_1}\left[M_1\frac{\mathrm{d}}{\mathrm{d}x}+jk\right](p_2-p_{2A})=0, \tag{31}$$

$$\left[\frac{\mathrm{d}^2}{\mathrm{d}x^2}+k^2\right]p_{2A}+j\frac{4D_1}{(D_2^2-D_1^2)\varsigma_1}(p_2-p_{2A})=0, \tag{32}$$

or in a matrix form of

$$\begin{bmatrix} D^2+\alpha_1 D+\alpha_2 & \alpha_3 D+\alpha_4\\ \alpha_5 D+\alpha_6 & D^2+\alpha_7 D+\alpha_8\end{bmatrix}\begin{bmatrix}p_2\\ p_{2A}\end{bmatrix}=\begin{bmatrix}0\\0\end{bmatrix}. \tag{33}$$

Developing Eq. (33) yields

$$\begin{aligned} p_2''+\alpha_1 p_2'+\alpha_2 p_2+\alpha_3 p_{2A}'+\alpha_4 p_{2A}&=0,\\ \alpha_5 p_2'+\alpha_6 p_2+p_{2A}''+\alpha_7 p_{2A}'+\alpha_8 p_{2A}&=0. \end{aligned} \tag{34}$$

Setting $p_2'=\frac{\mathrm{d}p_2}{\mathrm{d}x}=y_1$, $p_{2A}'=\frac{\mathrm{d}p_{2A}}{\mathrm{d}x}=y_2$, $p_2=y_3$, $p_{2A}=y_4$, it has

$$\begin{bmatrix}y_1'\\y_2'\\y_3'\\y_4'\end{bmatrix}=\begin{bmatrix}-\alpha_1 & -\alpha_3 & -\alpha_2 & -\alpha_4\\ -\alpha_5 & -\alpha_7 & -\alpha_6 & -\alpha_8\\ 1 & 0 & 0 & 0\\ 0 & 1 & 0 & 0\end{bmatrix}\begin{bmatrix}y_1\\y_2\\y_3\\y_4\end{bmatrix}. \tag{35}$$

Let

$$\{y\}=[\Omega]\{\Gamma\}, \tag{36}_1$$

where

$$\begin{bmatrix}\mathrm{d}p_2/\mathrm{d}x\\ \mathrm{d}p_{2A}/\mathrm{d}x\\ p_2\\ p_{2A}\end{bmatrix}=\begin{bmatrix}\Omega_{1,1} & \Omega_{1,2} & \Omega_{1,3} & \Omega_{1,4}\\ \Omega_{2,1} & \Omega_{2,2} & \Omega_{2,3} & \Omega_{2,4}\\ \Omega_{3,1} & \Omega_{3,2} & \Omega_{3,3} & \Omega_{3,4}\\ \Omega_{4,1} & \Omega_{4,2} & \Omega_{4,3} & \Omega_{4,4}\end{bmatrix}\begin{bmatrix}\Gamma_1\\ \Gamma_2\\ \Gamma_3\\ \Gamma_4\end{bmatrix}. \tag{36}_2$$

Let

$$[\chi]=[\Omega]^{-1}[N][\Omega]=\begin{bmatrix}\gamma_1 & 0 & 0 & 0\\ 0 & \gamma_2 & 0 & 0\\ 0 & 0 & \gamma_3 & 0\\ 0 & 0 & 0 & \gamma_4\end{bmatrix}. \tag{37}$$

The result is

$$\{\Gamma'\}=[\chi]\{\Gamma\}. \tag{38}$$

Plugging Eq. (38) into Eq. (36) yields

$$\begin{bmatrix}p_2(x)\\ p_{2A}(x)\\ \rho_o c_0 u_2(x)\\ \rho_o c_0 u_{2A}(x)\end{bmatrix}=\begin{bmatrix}H_{1,1} & H_{1,2} & H_{1,3} & H_{1,4}\\ H_{2,1} & H_{2,2} & H_{2,3} & H_{2,4}\\ H_{3,1} & H_{3,2} & H_{3,3} & H_{3,4}\\ H_{4,1} & H_{4,2} & H_{4,3} & H_{4,4}\end{bmatrix}\begin{bmatrix}k_1\\ k_2\\ k_3\\ k_4\end{bmatrix}. \tag{39}$$

Considering the boundary of $x = 0$ and $x = L_{C1}$ yields

$$\begin{bmatrix} p_2(0) \\ p_{2A}(0) \\ \rho_o c_0 u_2(0) \\ \rho_o c_0 u_{2A}(0) \end{bmatrix} = [\mathbf{H}(0)] \begin{bmatrix} k_1 \\ k_2 \\ k_3 \\ k_4 \end{bmatrix}, \quad \begin{bmatrix} p_2(L_C) \\ p_{2A}(L_C) \\ \rho_o c_0 u_2(L_C) \\ \rho_o c_0 u_{2A}(L_C) \end{bmatrix} = [\mathbf{H}(L_C)] \begin{bmatrix} k_1 \\ k_2 \\ k_3 \\ k_4 \end{bmatrix}. \tag{40}$$

Combining Eq. $(40)_1$ with Eq. $(40)_2$ yields

$$\begin{bmatrix} p_2(0) \\ p_{2A}(0) \\ \rho_o c_0 u_2(0) \\ \rho_o c_0 u_{2A}(0) \end{bmatrix} = [\mathbf{A}] \begin{bmatrix} p_2(L_C) \\ p_{2A}(L_C) \\ \rho_o c_0 u_2(L_C) \\ \rho_o c_0 u_{2A}(L_C) \end{bmatrix}. \tag{41}$$

Rearranging Eq. (41) yields

$$\begin{bmatrix} p_2(0) \\ \rho_o c_0 u_2(0) \end{bmatrix} = \begin{bmatrix} TP1_{1,1} & TP1_{1,2} \\ TP1_{2,1} & TP1_{2,2} \end{bmatrix} \begin{bmatrix} p_2(L_{C1}) \\ \rho_o c_0 u_2(L_{C1}) \end{bmatrix}, \tag{42}_1$$

or in the form of

$$\begin{bmatrix} p_2 \\ \rho_o c_0 u_2 \end{bmatrix} = \begin{bmatrix} TP1_{1,1} & TP1_{1,2} \\ TP1_{2,1} & TP1_{2,2} \end{bmatrix} \begin{bmatrix} p_3 \\ \rho_o c_0 u_3 \end{bmatrix}. \tag{42}_2$$

Subsequently, for the second perforated diffuser, the acoustical relationship within nodes 4, 5, 4A, and 5A is deduced as below:

- second inner tube:
  continuity equation

$$V \frac{\partial \rho_4}{\partial x'} + \rho_o \frac{\partial u_4}{\partial x'} + \frac{4\rho_o}{D_2} u_{u_2} + \frac{\partial \rho_4}{\partial t} = 0, \tag{43}$$

  momentum equation

$$\rho_o \left(\frac{\partial}{\partial t} + V_2 \frac{\partial}{\partial x'} \right) u_4 + \frac{\partial p_4}{\partial x'} = 0; \tag{42}$$

- second outer tube:
  continuity equation

$$\rho_o \frac{\partial u_{4A}}{\partial x'} - \frac{4 D_2 \rho_o}{D_3^2 - D_2^2} u + \frac{\partial \rho_{4A}}{\partial t} = 0, \tag{44}$$

  momentum equation

$$\rho_o \frac{\partial u_{4A}}{\partial t} + \frac{\partial p_{4A}}{\partial x'} = 0. \tag{45}$$

Similarly, as derived in Eqs (26)–(42), the four-pole matrix between nodes 4 and 5 yields

$$\begin{bmatrix} p_4(0) \\ \rho_o c_0 u_4(0) \end{bmatrix} = \begin{bmatrix} TP2_{1,1} & TP2_{1,2} \\ TP2_{2,1} & TP2_{2,2} \end{bmatrix} \begin{bmatrix} p_4(L_{C2}) \\ \rho_o c_0 u_4(L_{C2}) \end{bmatrix}, \tag{46}_1$$

or in the form of

$$\begin{bmatrix} p_4 \\ \rho_o c_0 u_4 \end{bmatrix} = \begin{bmatrix} TP2_{1,1} & TP2_{1,2} \\ TP2_{2,1} & TP2_{2,2} \end{bmatrix} \begin{bmatrix} p_5 \\ \rho_o c_0 u_5 \end{bmatrix}. \tag{46}_2$$

References

1. Bie D.A., Hansen C.H. (1988), *Engineering Noise Control: Theory and Practice*, Unwin Hyman, London.
2. Chang Y.C., Yeh L.J., Chiu M.C. (2004), Numerical studies on constrained venting system with side inlet/outlet mufflers by GA optimization, *Acta Acustica united with Acustica*, **90**(6): 1159–1169.
3. Chang Y.C., Yeh L.J., Chiu M.C. (2005a), Shape optimization on double-chamber mufflers using genetic algorithm, *Proceedings of the Institution of Mechanical Engineers, Part C: Journal of Mechanical Engineering Science*, **219**(1): 31–42, doi: 10.1243/095440605X8351.
4. Chang Y.C., Yeh L.J., Chiu M.C., Lai G.J. (2005b), Shape optimization on constrained single-layer sound absorber by using GA method and mathematical gradient methods, *Journal of Sound and Vibration*, **1286**(4–5): 941–961, doi: 10.1016/j.jsv.2004.10.039.
5. Chiu M.C. (2009a), Optimization of equipment allocation and sound-barriers shape in a multi-noise plant by using simulated annealing, *Noise & Vibration Worldwide*, **40**(7): 23–35, doi: 10.1260/095745609788921857.
6. Chiu M.C. (2009b), Simulated annealing optimization on multi-chamber mufflers hybridized with perforated plug-inlet under space constraints, *Archives of Acoustics*, **34**(3): 305–343.
7. Chiu M.C. (2010a), Numerical optimization of a three-chamber muffler hybridized with a side inlet and a perforated tube by SA method, *Journal of Marine Science and Technology*, **18**(4): 484–495, doi: 10.51400/2709-6998.1897.
8. Chiu M.C. (2010b), Optimal design of multi-chamber mufflers hybridized with perforated intruding inlets and resonated tube using simulated annealing, *Journal of Vibration and Acoustics*, **132**(5): Article ID 054503, doi: 10.1115/1.4001514.
9. Chiu M.C. (2012), Noise elimination of a multi-tone broadband noise with hybrid Helmholtz mufflers using a simulated annealing method, *Archives of Acoustics*, **37**(4): 489–498, doi: 10.2478/v10168-012-0061-0.
10. Chiu M.C. (2013), Numerical assessment for a broadband and tuned noise using hybrid mufflers and a simulated annealing method, *Journal of Sound and Vibration*, **332**(12): 2923–2940, doi: 10.1016/j.jsv.2012.12.039.
11. Chiu M.C. (2014a), Acoustical treatment of multi-tone broadband noise with hybrid side-branched mufflers using a simulated annealing method, *Journal of Low Frequency Noise Vibration and Active Control*, **33**(1): 79–112, doi: 10.1260/0263-0923.33.1.79.
12. Chiu M.C. (2014b), Optimal design on one-layer close-fitting acoustical hoods using a simulated annealing method, *Journal of Marine Science and Technology*, **22**(2): 211–217, doi: 10.6119/JMST-013-0503-1.
13. Chiu M.C., Chang Y.C. (2014), An assessment of high-order-mode analysis and shape optimization

of expansion chamber mufflers, *Archives of Acoustics*, **39**(4): 489–499, doi: 10.2478/aoa-2014-0053.

14. Kirkpatrick S., Gelatt C.D., Vecchi M.P. (1983), Optimization by simulated annealing, *Science*, **220** (4598): 671–680, doi: 10.1126/science.220.4598.671.
15. Metropolis A., Rosenbluth W., Rosenbluth M.N., Teller H., Teller E. (1953), Equation of static calculations by fast computing machines, *The Journal of Chemical Physics*, **21**(6): 1087–1092, doi: 10.1063/1.1699114.
16. Munjal M.L. (1987), *Acoustics of Ducts and Mufflers with Application to Exhaust and Ventilation System Design*, John Wiley & Sons, New York.
17. Munjal M.L., Rao K.N., Sahasrabudhe A.D. (1987), Aeroacoustic analysis of perforated muffler components, *Journal of Sound and Vibration*, **114**(2): 173–188, doi: 10.1016/S0022-460X(87)80146-3.
18. Peat K.S. (1988), A numerical decoupling analysis of perforated pipe silencer elements, *Journal of Sound and Vibration*, **123**(2), 199–212.
19. Sullivan J.W. (1979a), A method of modeling perforated tube muffler components I: theory, *The Journal of the Acoustic Society of America*, **66**(3): 772–778, doi: 10.1121/1.383679.
20. Sullivan J.W. (1979b), A method of modeling perforated tube muffler components II: theory, *The Journal of the Acoustic Society of America*, **66**(3): 779–788, doi: 10.1121/1.383680.
21. Sullivan J.W., Crocker M.J. (1978), Analysis of concentric tube resonators having unpartitioned cavities, *The Journal of the Acoustic Society of America*, **64**(1): 207–215, doi: 10.1121/1.381963.
22. Yeh L.J., Chang Y.C., Chiu M.C., Lai G.J. (2004), GA optimization on multi-segments muffler under space constraints, *Applied Acoustics*, **65**(5): 521–543, doi: 10.1016/j.apacoust.2003.10.010.
23. Yeh L.J., Chang Y.C., Chiu M.C. (2006), Numerical studies on constrained venting system with reactive mufflers by GA optimization, *International Journal for Numerical Methods in Engineering*, **65**(8): 1165–1185, doi: 10.1002/nme.1476.